Catalysis Communications 153 (2021) 106302

Contents lists available at ScienceDirect

Catalysis Communications

journal homepage: www.elsevier.com/locate/catcom

Short communication

Ordered macroporous Co_3O_4-supported Ru nanoparticles: A robust catalyst for efficient hydrodeoxygenation of anisole

An Wang, Yisheng Shi, Lan Yang *, Guoli Fan, Feng Li *

State Key Laboratory of Chemical Resource Engineering, Beijing Advanced Innovation Center for Soft Matter Science and Engineering, Beijing University of Chemical Technology, Beijing 100029, China

ARTICLE INFO

Keywords:
Ordered macroporous Co_3O_4
Defective structure
Highly dispersed Ru species
Hydrodeoxygenation
Biomass conversion

ABSTRACT

A three-dimensional ordered macroporous Co_3O_4 (OM-Co_3O_4) supported Ru catalyst was developed for the efficient hydrodeoxygenation (HDO) of anisole. It is revealed that small-sized Ru nanoparticles evenly distributed over the surface of OM-Co_3O_4 with large quantities of oxygen vacancies could strongly capture Ru^0 species, thereby resulting in strong Ru-Co_3O_4 interactions. Compared with commercial Co_3O_4 supported Ru catalyst, Ru/OM-Co_3O_4 displays a better catalytic HDO performance, with a high cyclohexane yield of 92.4% at 250 °C and 0.5 MPa hydrogen pressure after 5 h on stream. Such a significant efficiency of Ru/OM-Co_3O_4 is mainly attributed to both high dispersion of Ru^0 species and an enhanced formation of surface defects, as well as the unique macroporous framework of OM-Co_3O_4 support.

1. Introduction

Nowadays, the increasing environmental pollution and emissions of greenhouse gases stemming from the fast depletion of fossil resources imposed an increasing attention for developing efficient transformations of abundant and renewable lignin-based biomass resources. In this regard, lignin derivatives can be converted into high value-added chemicals and biofuels through the catalytic hydrodeoxygenation (HDO) process to partly replace at least non-renewable fossil resources [1–3]. For instance, anisole is often considered as a representative model substrate of lignin derivatives. For the catalytic HDO of anisole, due to their high catalytic activity, numerous metal oxides supported noble metal heterogeneous catalysts (e.g., Ru [4,5], Re [6], Pd [7], and Pt [8]) were widely explored. In addition, some transition metals and metal phosphides (e.g., Ni [9], Mo [10], CoMo [11], and Ni_2P [12]) were investigated. Despite the high selectivities to deoxygenated products obtained, HDO processes are usually conducted under harsh reaction conditions, namely: high reaction temperatures ($T > 250$ °C), high hydrogen pressure (3–6 MPa), and high metal loading amounts. Additionally, there exist some disadvantages of high catalyst cost and difficulty in catalyst reusability in some cases. Therefore, despite numerous research efforts, it is a huge challenge to develop highly efficient heterogeneous catalysts for the HDO of lignin derivatives.

On the other hand, reducible Co_3O_4 is often used as a heterogeneous catalytic material [13,14]. Specifically, surface defects on reducible Co_3O_4 may benefit the activation of oxygen-containing functional groups, thereby promoting the catalytic performance of Co_3O_4-based catalysts. Recently, metal oxide-based macroporous materials have been applied in the fields of adsorption and catalysis (e.g., environmentally benign oxidation of volatile organic compounds [15,16]), because of their higher porosity and mass transfer rates, and larger concentration of surface defects, in comparison to bulk materials. However, there have been no reports on the development of macroporous Co_3O_4 supported noble metal catalysts for catalytic hydrogenation applications.

In this communication, we fabricated a new three-dimensional (3D) ordered macroporous Co_3O_4-supported Ru catalyst (Ru/OM-Co_3O_4). Subsequently, he latter catalytic structure was investigated in the HDO of anisole under mild reaction conditions (i.e., 250 °C and 0.5 MPa hydrogen pressure). For comparison, the HDO reaction was also performed over Ru supported on other 3D ordered macroporous NiO and Al_2O_3 structures (OM-NiO and OM-Al_2O_3). The results showed that the present Ru/OM-Co_3O_4 catalyst could attain a much higher cyclohexane selectivity of 92.4% at a complete anisole conversion, compared with the commercial Co_3O_4, OM-NiO and OM-Al_2O_3 supported catalysts. The high catalytic efficiency of Ru/OM-Co_3O_4 was associated with both the beneficial activation of oxygen-containing groups in anisole at the surface oxygen vacancies of the OM-Co_3O_4 support, and the presence of highly dispersed Ru NPs, as well as the full exposure of active reaction/

* Corresponding author.
E-mail addresses: yanglan@mail.buct.edu.cn (L. Yang), lifeng@mail.buct.edu.cn (F. Li).

https://doi.org/10.1016/j.catcom.2021.106302
Received 23 November 2020; Received in revised form 6 March 2021; Accepted 8 March 2021
Available online 10 March 2021

adsorption sites and favorable mass transfer related to the ordered macroporous structure of OM-Co_3O_4 support.

2. Experimental

2.1. Catalysts synthesis

Polymethyl methacrylate (PMMA) template beads were prepared by emulsion polymerization [17]. OM-Co_3O_4 support was fabricated by a sacrificial hard template method, and the resulting OM-Co_3O_4 supported Ru sample having a Ru loading of about 1.1 wt% was synthesized by the liquid-phase reduction process using sodium borohydride as reductant (see details in the Electronic Supporting Information, ESI). Other 3D ordered macroporous NiO and Al_2O_3 (denoted as OM-NiO or OM-Al_2O_3) and resulting supported Ru catalyst samples were synthesized according to identical procedures to those for OM-Co_3O_4 and Ru/OM-Co_3O_4 samples.

2.2. Sample characterizations

Samples were characterized by X-ray diffraction (XRD), scanning electron microscopy (SEM), transmission electron microscopy (TEM), X-ray photoelectron spectroscopy (XPS), H_2 temperature programmed desorption (H_2-TPD), H_2 temperature programmed reduction (H_2-TPR), and Raman spectroscopy (see details in the Electronic Supporting Information, ESI).

2.3. Catalytic HDO tests

Details of catalytic HDO tests are included in the Electronic Supporting Information (ESI).

3. Results and discussion

3.1. Sample characterization

As presented in Fig. S1 (ESI), XRD patterns for Ru/OM-Co_3O_4 sample exhibit several diffraction peaks, which match well those of the cubic Co_3O_4 spinel phase (JCPDS 42–1467). No diffractions corresponding to metallic Ru^0 phase were observed, mainly owing to the small size (< 4 nm) of Ru^0 particles and the low Ru loading used (~ 1.1 wt%) determined by ICP-AES analysis. The results reflect the good dispersion of Ru species on the surface of OM-Co_3O_4 support. As shown in Fig. S2 (ESI), Ru/OM-Co_3O_4 displays a 3D honeycomb-like ordered macroporous structure, in which hollow spheres are interconnected together through walls. TEM images of Ru/OM-Co_3O_4 (Fig. 1) depict that the large quantities of small Ru NPs with an average diameter of ~2.53 nm are uniformly attached on the surface of a nearly uniform OM-Co_3O_4 support, thereby forming the close interface between them. This is well consistent with the powder XRD results. Meanwhile, one can discern the lattice fringes of the (101) and (511) crystal facets of Ru^0 and Co_3O_4 phases with facet spacing of 0.206 and 0.155 nm, respectively. In this case, both the ordered macroporous framework of OM-Co_3O_4 and the high dispersion of Ru NPs may favor full exposure of the adsorption and reaction active sites. In contrast, in addition to a few aggregates of particles, larger Ru particles with the size of ~15–20 nm are found to be distributed over the surface of the commercial Co_3O_4- supported Ru sample (Fig. S3, ESI). The above results illustrate that OM-Co_3O_4 support shows a promotional effect on the improvement of the dispersion of Ru and the formation of smaller Ru NPs.

The structural defects can be easily generated through calcination or reduction treatments during the synthesis of supported catalysts, and further promote their catalytic performance of catalysts [18,19]. Therefore, XPS characterization was performed to identify surface electronic states of metal and oxygen species on Ru-based samples (Fig. 2). In the XPS of Ru $3d_{5/2}$ region for the Ru/OM-Co_3O_4 and Ru/Co_3O_4 samples, a peak with a binding energy at ~280.3 eV is observed, minoring the presence of metallic Ru^0 species (Fig. S4, ESI). In the deconvoluted Co 2p region, Co $2p_{3/2}$ and Co $2p_{1/2}$ core levels appear at 777–785 and 792.5–801 eV, respectively, indicative of the presence of Co^{2+} and Co^{3+} species [20]. Notably, the surface fraction of Co^{2+} in the total Co species on the Ru/OM-Co_3O_4 (0.51) is larger than that on Ru/Co_3O_4 (0.42), reflecting the formation of more defective Co^{2+} sites. Meanwhile, XPS of the O 1 s region depicts the existence of three kinds of oxygen species at ~529.6, 531.3 and 532.8 eV, respectively, which correspond to lattice oxygen (O_I), oxygen species adsorbed on defects (e.g., oxygen vacancies) or hydroxyl species (O_{II}), and surface carbonate ions (O_{III}) [21]. Noticeably, the surface $O_{II}/(O_I + O_{II} + O_{III})$ fraction on the Ru/OM-Co_3O_4 (0.48) is higher than that on the Ru/Co_3O_4 (0.41), likely suggestive of the generation of more oxygen vacancies.

Raman spectra provide insight into the defective crystal structures. As illustrated in Fig. S5 (ESI), compared with those for Ru/Co_3O_4, five characteristic Raman peaks (F^1_{2g}, E_{2g}, F^2_{2g}, F^3_{2g}, and A_{1g}) of Co_3O_4 phase for the Ru/OM-Co_3O_4 solid all shift to low frequencies at the 532-nm laser wavelength, despite the reduced peak intensities. These results demonstrate the presence of lattice distortion/strain of Co_3O_4 spinel phase, and thus the formation of more Co^{2+}-O_v-Co^{2+} like structural defects (O_v: oxygen vacancies) in the vicinity of Co^{2+} species on the Ru/OM-Co_3O_4 [22,23], mainly thanks to the multiple calcination processes conducted during the synthesis of OM-Co_3O_4.

3.2. Catalytic HDO performance of supported Ru catalysts

Fig. 3 shows the variation of anisole conversion and product distribution with reaction time after HDO reaction at 250 °C and 0.5 MPa over the Ru/OM-Co_3O_4 catalyst. The main deoxygenated products are

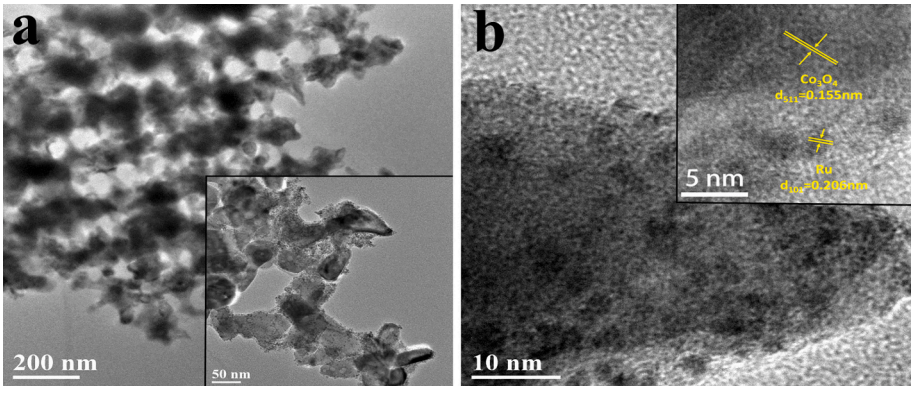

Fig. 1. TEM (a) and high-resolution TEM (b) images of Ru/OM-Co_3O_4 catalyst sample. Insets in (a) and (b) show the macroporous network structure and the lattice fringes of Ru^0 and Co_3O_4 phases, respectively.

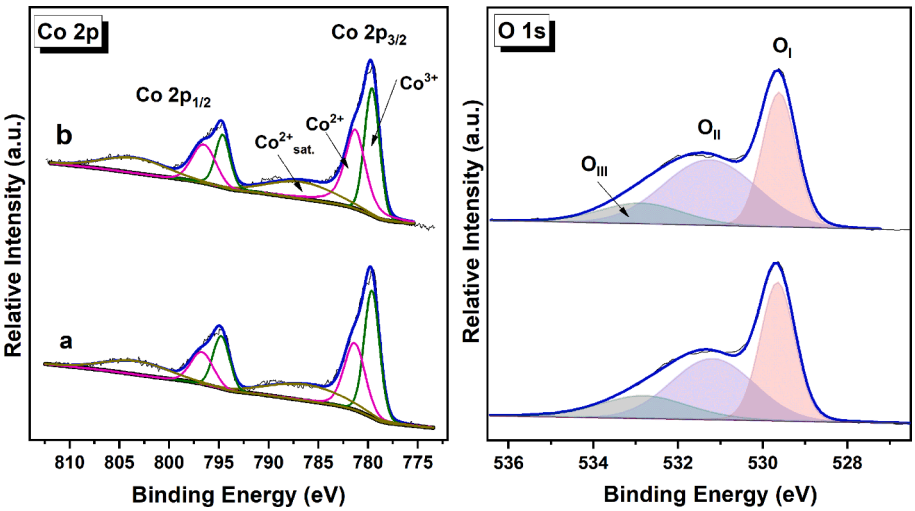

Fig. 2. XPS of Co 2p and O 1 s regions of Ru/Co_3O_4 (a) and $Ru/OM\text{-}Co_3O_4$ (b) catalyst samples.

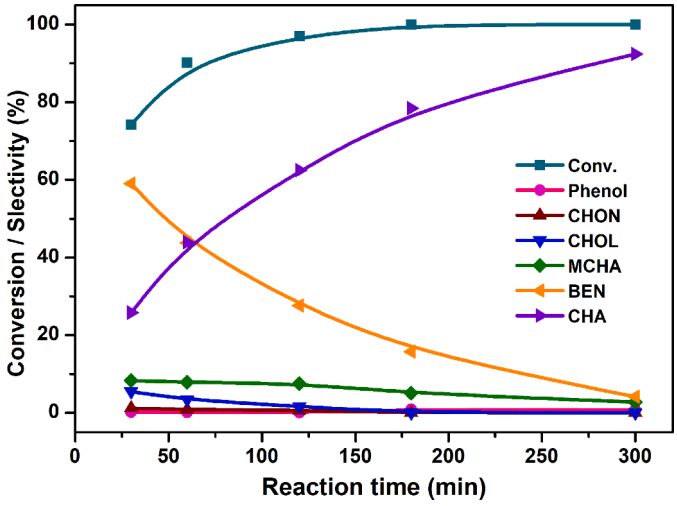

Fig. 3. Conversion and product selectivities profiles with reaction time over the $Ru/OM\text{-}Co_3O_4$ catalyst. Reaction conditions: 0.5 MPa hydrogen pressure; 250 °C.

benzene (BEN) and cyclohexane (CHA), along with the formation of small amounts of methoxycyclohexane (MCHA) and cyclohexanol (CHOL) by-products, and trace amounts of cyclohexanone (CNON) and phenol. With prolonged reaction time, the benzene selectivity gradually decreases, whereas the cyclohexane selectivity progressively increases. Besides a small amount of benzene with a yield of 4.2%, a large amount of cyclohexane with a high yield of 92.4% is obtained at complete conversion after 5 h of reaction. Over the pure $OM\text{-}Co_3O_4$ support, almost no conversion of anisole was obtained. As shown in Table 1 (entry 1), Ru/Co_3O_4 exhibits a low catalytic activity for the HDO reaction with a much lower conversion, ca. 38.3% and a lower selectivity to deoxygenated products (ca. 66.3%) after 1 h. Notably, compared to Ru/Co_3O_4, the catalytic HDO performance of $Ru/OM\text{-}Co_3O_4$ is significantly improved, along with high conversion (90.2%) and selectivity to deoxygenated products (87.7%) (Table 1, entry 2). Compared with $Ru/OM\text{-}Co_3O_4$, the other two Ru/OM-NiO and $Ru/OM\text{-}Al_2O_3$ reference catalysts deliver lower conversions and selectivity to deoxygenated products (Table 1, entries 3 and 4).

Since the activity and selectivity to deoxygenation products over the Ru/Co_3O_4 are much inferior to those over the $Ru/OM\text{-}Co_3O_4$ catalyst in the HDO process, one can confirm that surface Ru species and $OM\text{-}Co_3O_4$ support should play important roles in controlling the HDO process of anisole. In the present $Ru/OM\text{-}Co_3O_4$ catalyst, $OM\text{-}Co_3O_4$ support with a higher surface area of 24.3 m^2/g can effectively serve as a support for achieving higher dispersion of small-sized Ru NPs, compared with the commercial Co_3O_4 with smaller specific surface area, ca. 4.5 m^2/g. Further, TEM observations reveal the formation of highly dispersed and small-sized Ru NPs on the $OM\text{-}Co_3O_4$, which greatly facilitate the accessibility of active metallic Ru sites to substrates, and thus the dissociation of molecular hydrogen. Meanwhile, XPS and Raman results demonstrate the presence of more defects on $Ru/OM\text{-}Co_3O_4$, in comparison to Ru/Co_3O_4. Furthermore, the present Co_3O_4-supported Ru catalysts should be activated by H_2 at high temperature before testing, and correspondingly the Co_3O_4 support could be reduced partly, as evidenced by the XPS analysis of the used catalysts (Fig. S6, ESI), thus leading to the increased surface $Co^{2+}/(Co^{2+}+Co^{3+})$ ratio (0.56 for $Ru/OM\text{-}Co_3O_4$ and 0.47 for Ru/Co_3O_4), and the O_{II} fraction (0.65 for $Ru/OM\text{-}Co_3O_4$ and 0.5 for Ru/Co_3O_4) after the HDO reaction. Such abundant surface defective structures probably lead to the easier activation of methoxy group in anisole through the interaction between defective Co^{2+} species and oxygen atom of the methoxy group, and thus direct deoxygenation process to form benzene [5]. Subsequently, a further ring-hydrogenation of benzene can produce cyclohexane.

In this work, we further carried out H_2-TPD experiments to determine the ability of H_2 dissociation and the occurrence of hydrogen

Table 1
Comparison of different catalysts for HDO of anisole. [a]

Catalysts	Conv. (%)	Selectivity (%)					
		Phenol	CHON	CHOL	MOCHN	Benzene	CHA
$Ru/OM\text{-}Co_3O_4$	90.2	0.1	0.9	3.4	7.9	43.8	43.9
Ru/Co_3O_4	38.3	0	2.4	12.4	18.9	47.4	18.9
Ru/OM-NiO	85.4	0	0.9	3.7	33.5	24.3	37.6
$Ru/OM\text{-}Al_2O_3$	11.3	2.4	8.5	19.8	23.8	39.1	6.4

[a] Reaction conditions: 20 mg catalyst, 0.22 mL anisole, 250 °C, 0.5 MPa hydrogen pressure, and 1 h reaction time.

spillover on Ru-based catalyst samples. As presented in Fig. S7 (ESI), in the case of Ru/OM-Co_3O_4 sample, two desorption peaks located at ~92 and 300 °C correspond to desorption of hydrogen from Ru particles and highly dispersed Ru species strongly interacting with the support, respectively. The desorption peak at 535 °C is assigned to spillover hydrogen adsorbed on the support [24,25]. In contrast, no hydrogen spillover occurs on the Ru/Co_3O_4, besides a remarkably reduced desorption originating from the absence of highly dispersed Ru species. What's more, H_2-TPR traces display that compared to pure OM-Co_3O_4 (386 and 501 °C, respectively), Ru/OM-Co_3O_4 exhibits lower reduction temperatures for Co^{3+} to Co^{2+} and Co^{2+} to Co^0 species (360 and 489 °C, respectively, Fig. S8, ESI), confirming the occurrence of a much stronger hydrogen spillover from highly dispersed Ru^0 species on the Co_3O_4 surface of the Ru/OM-Co_3O_4 catalyst.

Therefore, thanks to the highly dispersive character of Ru species on the OM-Co_3O_4 support, and its abundant defective structure, both H_2 dissociation and hydrogen spillover take place more easily on the Ru/OM-Co_3O_4 than on the Ru/Co_3O_4, thereby, significantly improving the catalytic HDO performance of Ru/OM-Co_3O_4. Also, the unique macroporous structure of OM-Co_3O_4 support provide a large number of open channels, which may likely favor the exposure of active reaction/adsorption sites and the facile diffusion of reactants and products, thereby promoting the catalytic HDO performance of Ru/OM-Co_3O_4 to some extent. It can be concluded that the higher catalytic performance of Ru/OM-Co_3O_4 should be closely associated with the surface cooperation between highly dispersed Ru NPs and defective sites present in the OM-Co_3O_4 support, as well as the unique macroporous framework of OM-Co_3O_4 support.

The influence of reaction temperature and hydrogen pressure on the HDO of anisole was also investigated over the Ru/OM-Co_3O_4 catalytic system. As presented in Fig. S9 (ESI), with the elevated reaction temperature from 200 to 275 °C, the anisole conversion gradually increases from 42.5 to 98.6%, while the selectivity to deoxygenated products (benzene and cyclohexane) progressively increases from 44.7 to 94.7%. These results demonstrate that the high reaction temperature can promote the HDO of anisole. Fig. S10 (ESI) shows that benzene selectivity becomes quite low (<1.0%) above 1.0 MPa of hydrogen pressure. This is because the high hydrogen pressure favors the hydrogenation of benzene ring to form methoxycyclohexane and cyclohexane, thus inhibiting the direct cleavage of the methoxy group to form benzene. As summarized in Table S1 (ESI), compared to Ru-based catalysts previously reported, the present Ru/OM-Co_3O_4 catalytic system possesses better or at least comparative catalytic performance in the anisole HDO under mild reaction conditions.

The stability of heterogeneous catalysts is one of the key indexes for their practical application. As displayed in Fig. 4, the selectivity to each product is almost unchanged, and the conversion is only decreased by ~1.3% after five successive HDO tests using the Ru/OM-Co_3O_4 catalytic system. Further, SEM and TEM images of the used catalyst (Fig. S11, ESI) reveal that the macroporous structure of OM-Co_3O_4 is kept unchanged, and no structural collapse occurs. It is indicated that Ru/OM-Co_3O_4 catalyst has good structural stability and reusability, mainly thanks to the strong interactions developed between Ru NPs and OM-Co_3O_4 support.

4. Conclusions

In summary, we synthesized a new supported Ru catalyst on the OM-Co_3O_4 carrier, and utilized the OM-Co_3O_4 with appropriate surface defects to enhance the dispersion of small-sized Ru nanoparticles and create strong metal-support interactions. The Ru/OM-Co_3O_4 could afford a 92.4% yield of cyclohexane in the anisole HDO under mild reaction conditions (0.5 MPa hydrogen pressure and 250 °C), indicative of high activity and selectivity to deoxygenated products (benzene and cyclohexane). The formation of highly dispersed Ru species and more surface defects could favor the adsorption and activation of reactants on the catalyst surface. A significant diffusion behavior of reactants and products originating from the unique macroporous framework structure of OM-Co_3O_4 is very likely to account for the high catalytic efficiency of Ru/OM-Co_3O_4. It is expected that the present reported approach using OM-Co_3O_4 as catalyst support is novel and reproducible, and would be a promising approach for designing other high-performance supported catalysts applied in several other heterogeneous catalytic processes.

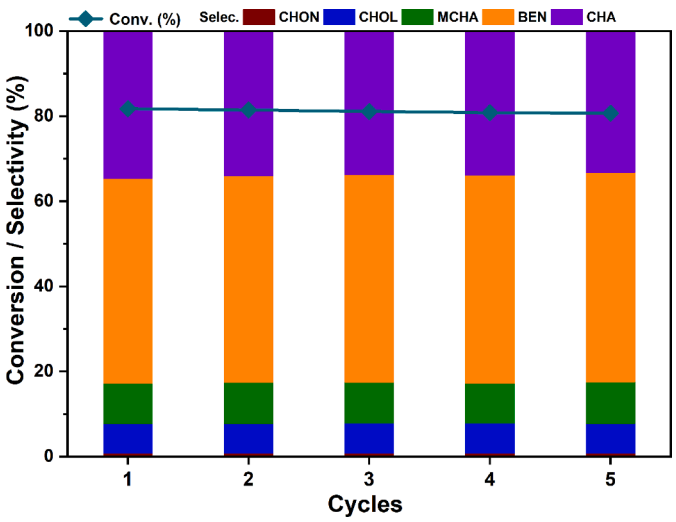

Fig. 4. Conversion and product selectivities with number of recycling runs over the Ru/OM-Co_3O_4 catalyst. Reaction conditions: 0.5 MPa hydrogen pressure; 250 °C;1 h reaction time.

Declaration of Competing Interest

The authors declare that they have no known competing financial interests or personal relationships that could have appeared to influence the work reported in this paper.

Acknowledgments

We gratefully thank the National Natural Science Foundation of China (21776017;21991102; U19B6002) for financial support.

Appendix A. Supplementary data

Supplementary data to this article can be found online at https://doi.org/10.1016/j.catcom.2021.106302.

References

[1] Q. Tan, G. Wang, A. Long, A. Dinse, C. Buda, J. Shabaker, D.E. Resasco, Mechanistic analysis of the role of metal oxophilicity in the hydrodeoxygenation of anisole, J. Catal. 347 (2017) 102–115, https://doi.org/10.1016/j.jcat.2017.01.008.

[2] J. Zhang, B. Fidalgo, A. Kolios, D. Shen, S. Gu, Mechanism of deoxygenation in anisole decomposition over single-metal loaded HZSM-5: experimental study, Chem. Eng. J. 336 (2018) 211–222, https://doi.org/10.1016/j.cej.2017.11.128.

[3] T.M. Sankaranarayanan, A. Berenguer, C. Ochoa-Hernández, I. Moreno, P. Jana, J. M. Coronado, D.P. Serrano, P. Pizarro, Hydrodeoxygenation of anisole as bio-oil model compound over supported Ni and Co catalysts: effect of metal and support properties, Catal. Today 243 (2015) 163–172, https://doi.org/10.1016/j.cattod.2014.09.004.

[4] T.N. Phan, Y.K. Park, I.G. Lee, C.H. Ko, Enhancement of Csingle bondO bond cleavage to afford aromatics in the hydrodeoxygenation of anisole over ruthenium-supporting mesoporous metal oxides, Appl. Catal. A Gen. 544 (2017) 84–93, https://doi.org/10.1016/j.apcata.2017.06.029.

[5] T.N. Phan, C.H. Ko, Synergistic effects of Ru and Fe on titania-supported catalyst for enhanced anisole hydrodeoxygenation selectivity, Catal. Today 303 (2018) 219–226, https://doi.org/10.1016/j.cattod.2017.08.025.

[6] I.T. Ghampson, G. Pecchi, J.L.G. Fierro, A. Videla, N. Escalona, Catalytic hydrodeoxygenation of anisole over re-MoO_x/TiO_2 and re-VO_x/TiO_2 catalysts,

Appl. Catal. B Environ. 208 (2017) 60–74, https://doi.org/10.1016/j.apcatb.2017.02.047.
[7] D.P. Gamliel, S. Karakalos, J.A. Valla, Liquid phase hydrodeoxygenation of anisole, 4-ethylphenol and benzofuran using Ni, Ru and Pd supported on USY zeolite, Appl. Catal. A Gen. 559 (2018) 20–29, https://doi.org/10.1016/j.apcata.2018.04.004.
[8] D. Shi, L. Arroyo-Ramírez, J.M. Vohs, The use of bimetallics to control the selectivity for the upgrading of lignin-derived oxygenates: reaction of anisole on Pt and PtZn catalysts, J. Catal. 340 (2016) 219–226, https://doi.org/10.1016/j.jcat.2016.05.020.
[9] H. Taghvaei, M.R. Rahimpour, P. Bruggemanc, Catalytic hydrodeoxygenation of anisole over nickel supported on plasma treated alumina–silica mixed oxides, RSC Adv. 7 (2017) 30990–30998, https://doi.org/10.1039/C7RA02594G.
[10] B. Rahzani, M. Saidi, H.R. Rahimpour, B.C. Gatesc, M.R. Rahimpour, Experimental investigation of upgrading of lignin-derived bio-oil component anisole catalyzed by carbon nanotube-supported molybdenum, RSC Adv. 7 (2017) 10545–10556, https://doi.org/10.1039/C6RA26121C.
[11] D. Otyuskaya, J.W. Thybaut, R. Løndeng, G.B. Marin, Anisole Hydrotreatment kinetics on CoMo catalyst in the absence of Sulfur: experimental investigation and model construction, Energy Fuel 31 (2017) 7082–7092, https://doi.org/10.1021/acs.energyfuels.7b00519.
[12] Y. Li, J. Fu, B. Chen, Highly selective hydrodeoxygenation of anisole, phenol and guaiacol to benzene over nickel phosphide, RSC Adv. 7 (2017) 15272–15277, https://doi.org/10.1039/C7RA00989E.
[13] X. Yang, J. Chen, Y. Chen, P. Feng, H. Lai, J. Li, X. Luo, Novel Co_3O_4 nanoparticles/nitrogen-doped carbon composites with extraordinary catalytic activity for oxygen evolution reaction (OER), Nano-Micro Lett. 10 (2018) 15, https://doi.org/10.1007/s40820-017-0170-4.
[14] X. Ma, X. Yu, X. Yang, M. Lin, M. Ge, Hydrothermal synthesis of a novel double-sided Nanobrush Co_3O_4 catalyst and its catalytic performance for benzene oxidation, ChemCatChem 11 (2019) 1214–1221, https://doi.org/10.1002/cctc.201801539.
[15] Z. Wang, X. Fan, D. Han, F. Gu, Structural and electronic engineering of 3DOM WO_3 by alkali metal doping for improved NO_2 sensing performance, Nanoscale 8 (2016) 10622–10631, https://doi.org/10.1039/C6NR00858E.
[16] Y. Cheng, W. Song, J. Liu, Z. Zhao, Y. Wei, Simultaneous removal of PM and NOx over highly efficient 3DOM $W/Ce_{0.8}Zr_{0.2}O_2$ catalysts, RSC Adv. 7 (2017) 56509–56518, https://doi.org/10.1039/C7RA11571G.
[17] Z. Wang, H. Zhou, D. Han, F. Gu, Electron compensation in p-type 3DOM NiO by Sn doping for enhanced formaldehyde sensing performance, J. Mater. Chem. C 5 (2017) 3254–3263, https://doi.org/10.1039/C7TC00226B.
[18] X. Pan, M.-Q. Yang, X. Fu, N. Zhang, Y.-J. Xu, Defective TiO_2 with oxygen vacancies: synthesis, properties and photocatalytic applications, Nanoscale 5 (2013) 3601–3614, https://doi.org/10.1039/c3nr00476g.
[19] M. Liu, J. Zhang, L. Zheng, G. Fan, L. Yang, F. Li, Significant promotion of surface oxygen vacancies on bimetallic CoNi nanocatalysts for hydrodeoxygenation of biomass-derived vanillin to produce Methylcyclohexanol, ACS Sustain. Chem. Eng. 8 (2020) 6075–6089, https://doi.org/10.1021/acssuschemeng.0c01015.
[20] X.H. Liu, L.J. Xu, G.Y. Xu, W.D. Jia, Y.F. Ma, Y. Zhang, Selective Hydrodeoxygenation of lignin-derived phenols to Cyclohexanols or Cyclohexanes over magnetic CoN_x@NC catalysts under mild conditions, ACS Catal. 6 (2016) 7611–7620, https://doi.org/10.1021/acscatal.6b01785.
[21] Q. Hu, L. Yang, G.L. Fan, F. Li, Hydrogenation of biomass-derived compounds containing a carbonyl group over a copper-based nanocatalyst: insight into the origin and influence of surface oxygen vacancies, J. Catal. 340 (2016) 184–195, https://doi.org/10.1016/j.jcat.2016.05.008.
[22] H. Yan, C.F. Blanford, B.T. Holland, W.H. Smyrl, A. Stein, General synthesis of periodic macroporous solids by templated salt precipitation and chemical conversion, Chem. Mater. 12 (2000) 1134–1141, https://doi.org/10.1021/cm9907763.
[23] X. Wang, Y. Liu, T. Zhang, Y. Luo, Z. Lan, K. Zhang, J. Zuo, L. Jiang, R. Wang, Geometrical-site-dependent catalytic activity of ordered mesoporous co-based spinel for benzene oxidation: in situ DRIFTS study coupled with Raman and XAFS spectroscopy, ACS Catal. 7 (2017) 1626–1636, https://doi.org/10.1021/acscatal.6b03547.
[24] Z. Gao, G. Fan, M. Liu, L. Yang, F. Li, Dandelion-like cobalt oxide microsphere-supported RuCo bimetallic catalyst for highly efficient Hydrogenolysis of 5-Hydroxymethylfurfural, Appl. Catal. B Environ. 237 (2018) 649–659, https://doi.org/10.1016/j.apcatb.2018.06.026.
[25] B. Lin, R. Li, R. Shu, C. Wang, Z. Yuan, Y. Liu, Y. Chen, Synergistic effect of highly dispersed Ru and moderate acid site on the Hydrodeoxygenation of phenolic compounds and raw bio-oil, J. Energy Inst. 93 (2020) 847–856, https://doi.org/10.1016/j.joei.2019.07.009.